# Modelling the unsteady melt flow under a pulsed magnetic field*

Chen Guo-Jun(陈国军)[a)†], Zhang Yong-Jie(张永杰)[b)], and Yang Yuan-Sheng(杨院生)[c)]

[a)] Key Laboratory of Electromagnetic Processing of Materials, Ministry of Education, Northeastern University, Shenyang 110819, China
[b)] Energy and Environmental Research Institute, Central Research Institute of Baosteel Group, Shanghai 201900, China
[c)] Institute of Metal Research, Chinese Academy of Sciences., Shenyang 110016, China

(Received 7 August 2013; revised manuscript received 24 September 2013)

A numerical model for the unsteady flow under a pulsed magnetic field of a solenoid is developed, in which magnetohydrodynamic flow equations decouple into a transient magnetic diffusion equation and unsteady Navier–Stokes equations in conjunction with two equations of the $k$–$\varepsilon$ turbulent model. A Fourier series method is used to implement the boundary condition of magnetic flux density under multiple periods of a pulsed magnetic field (PMF). The numerical results are compared with the theoretical or experimental results to validate the model under a time-harmonic magnetic field; it is found that the toroidal vortex pair is the dominating structure within the melt flow under a PMF. The velocity field of a molten melt is in a quasi-steady state after several periods; changing the direction of the electromagnetic force causes the vibration of the melt surface under a PMF.

**Keywords:** pulsed magnetic field, Fourier series, velocity field, turbulent model

**PACS:** 47.65.−d, 47.11.Df, 47.27.em, 02.30.Nw **DOI:** 10.1088/1674-1056/22/12/124703

## 1. Introduction

A pulsed magnetic field (PMF) has been proven to be a powerful method of changing the microstructure of casting ingots.[1–3] The magnetic-driven convection,[4] magnetic vibration,[5] and other effects[6] provoke distinct grain-refining effects, which improve the properties of casting under a PFM. According to coil structures of PMFs, they are classified as rotating PMF, traveling PMF, solenoid PMF, and combinations of these three PMFs. In this article, the PMF is only considered to be produced by means of a solenoid.

For optimizing the grain refining, a suitable magnetic field needs to be designed. Furthermore, the magnetic field parameters (amplitude, frequency and duty ratio) can be adjusted according to the requirements. Kolesnichenko *et al.*[7] simulated the magnetic force and the flow distribution under a PMF produced by a sine wave current in applying pulse time and offered optimization duration. Zu *et al.*[8] investigated the flow distribution under a strong PMF, showing that there is a double effect of electromagnetic stirring and vibration on the aluminum alloy melt under a PMF in the applied pulse time. To further investigate the variation of a whole pulse period, Ma *et al.*[9] simulated magnetic force and flow distribution under a PMF by half sine-wave during one whole period, showing that the magnetic pressure force and pull force appear alternately and produce the vibration of the melt and that the frequency of the PMF has no effect on the electromagnetic force.

In summary, MHD model approaches to the simulation of the melt flow under a PMF are usually subject to the following restrictions.

(i) Considering one period time. In general, the magnetic field intensity $\boldsymbol{B}$ is unaffected by flow velocity $\boldsymbol{U}$, because of magnetic Reynolds ($Re_{\mathrm{m}}$) numbers far less than one.[10] So it is clear that the electromagnetic force varying with time and space can be known, if this force is calculated during one whole period (including the applied pulse time and pulse intermittent time). However, the velocity field of melt liquid has various distributions in a previous period and the following period under the PMF.

(ii) Associated with the laminar model. Actually the Reynolds ($Re$) number is usually more than 2300, which belongs to turbulent flow above the numerical results, especially under a strong PMF.

So the model of melt flow must be built for understanding the unsteady velocity field of the melt, containing a turbulent model with multiple periods under the PFM. In this paper, we present an unsteady melt flow model in order to simulate the velocity distribution under a PMF, including the $k$–$\varepsilon$ turbulent flow of the melt and the multiple pulse period at the same time. The approach of the Fourier series is used to calculate the electromagnetic force under multiple periods of a PMF. Using this model, we then present results for the electromagnetic force and unsteady melt flow distribution during multiple periods of a PMF.

## 2. Mathematical model

### 2.1. Physical model and parameter

The numerical model is assumed to be two-dimensional and axisymmetric. The geometry under investigation is shown

*Project supported by the National Natural Science Foundation of China (Grant No. 51034012).
†Corresponding author. E-mail: guojunchen_1984@163.com
© 2013 Chinese Physical Society and IOP Publishing Ltd 

in Fig. 1. A crucible contains the melt pool, which possesses a free surface. The liquid metal is driven by a time varying magnetic field $\boldsymbol{B}$.

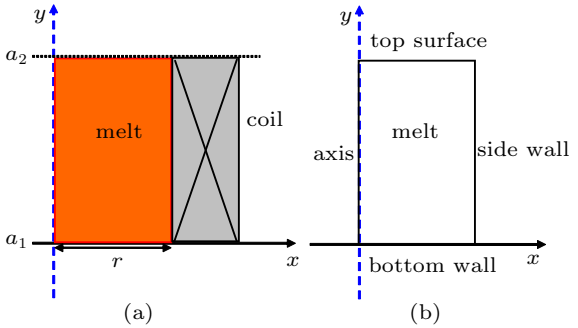



**Fig. 1.** (color online) Geometry sketch of numerical model (a) and boundary name (b).

### 2.2. Governing equations

The transport phenomena in a time-varying magnetic field are governed by the conservations of the mass, momentum, and magnetic diffusion of an incompressible, electrically conducting fluid.[10] Additionally, the turbulent flow is modeled through the use of the $k$–$\varepsilon$ model, where $k$ is the turbulent kinetic energy and $\varepsilon$ is the rate of dissipation of the kinetic energy. The Lorentz force is incorporated into Navier–Stokes equations. According to Maxwell stresses definition, the Lorentz force can be rewritten into $(B\cdot\nabla)(B/\mu_{\rm m})$ and $-\nabla(B^2/2\mu_{\rm m})$.

The continuity equation and momentum equation are

$$\frac{\partial \overline{u}_i}{\partial x_i}=0, \tag{1}$$

$$\rho\Big(\frac{\partial \overline{u}_i}{\partial t}+\overline{u}_j\frac{\partial \overline{u}_i}{\partial x_j}\Big)=-\frac{\partial \overline{p}}{\partial x_i}+(\mu_0+\mu_{\rm t})\frac{\partial^2 \overline{u}_i}{\partial x_j^2}+\frac{1}{\mu_{\rm m}}B_j\frac{\partial B_i}{\partial x_j}-\frac{1}{2\mu_{\rm m}}\frac{\partial B_i^2}{\partial x_i}, \tag{2}$$

where $\mu_{\rm t}=c_\mu k^2/\varepsilon$ is the turbulent viscosity, with $c_\mu=0.09$; $\mu_0$ is the molar viscosity; $\mu_{\rm m}$ is the magnetic permeability; and $i$ and $j$ represent the $x$ and $y$ coordinates.

The equation of the turbulent model[11] is

$$\frac{\partial(\rho k)}{\partial t}+\rho\overline{u}_j\frac{\partial k}{\partial x_j}=\frac{\partial}{\partial x_j}\Big[\Big(\mu+\frac{\mu_{\rm t}}{\sigma_{\rm k}}\Big)\frac{\partial k}{\partial x_j}\Big]+\mu_{\rm t}\frac{\partial \overline{u}_i}{\partial x_k}\Big(\frac{\partial \overline{u}_i}{\partial x_k}+\frac{\partial \overline{u}_k}{\partial x_j}\Big)-\rho\varepsilon, \tag{3}$$

$$\frac{\partial(\rho\varepsilon)}{\partial t}+\rho\overline{u}_j\frac{\partial \varepsilon}{\partial x_j}=\frac{\partial}{\partial x_j}\Big[\Big(\mu+\frac{\mu_{\rm t}}{\sigma_\varepsilon}\Big)\frac{\partial \varepsilon}{\partial x_j}\Big]+\frac{c_1\varepsilon}{k}\mu_{\rm t}\frac{\partial \overline{u}_i}{\partial x_k}\Big(\frac{\partial \overline{u}_i}{\partial x_k}+\frac{\partial \overline{u}_k}{\partial x_j}\Big)-c_2\rho\frac{\varepsilon^2}{k}, \tag{4}$$

where the constants used in the equation for $k$ and $\varepsilon$ are

$$\sigma_k=1.0,\quad \sigma_\varepsilon=1.3,\quad c_1=1.44,\quad \text{and}\quad c_2=1.92.$$

The magnetic diffusion equation from the Maxwell equation is

$$\frac{\partial B_i}{\partial t}+\overline{u}_j\frac{\partial B_i}{\partial x_j}=\lambda_{\rm mag}\frac{\partial^2 B_i}{\partial x_j^2}+B_i\frac{\partial \overline{u}_j}{\partial x_i}, \tag{5}$$

$$\frac{\partial B_i}{\partial x_i}=0, \tag{6}$$

where $\lambda_{\rm mag}=(\mu_{\rm m}\sigma)^{-1}$ and $\sigma$ is the electrical conductivity of the fluid. When we assume that $Re_{\rm m}$ is less than one, the electrically conducting fluid motion has no effect on the magnetic field. So the magnetic diffusion equation now becomes

$$\frac{\partial B_i}{\partial t}=\lambda_{\rm mag}\frac{\partial^2 B_i}{\partial x_j^2}, \tag{7}$$

$$\frac{\partial B_i}{\partial x_i}=0. \tag{8}$$

### 2.3. Boundary condition

A no-slip condition is applied at the bottom wall and side wall and a no-shear condition is imposed on the free surface. The boundary conditions are given in Table 1.

**Table 1.** Boundary conditions for melt flow under PMF.

| Top | Bottom | Side wall | axis |
|---|---|---|---|
| $\overline{u}_y=0$ | $\overline{u}_x=0$ | $\overline{u}_x=0$ | $\overline{u}_x=0$ |
| $\frac{\partial B_y}{\partial y}=0$ | $\overline{u}_y=0$ | $\overline{u}_y=0$ | $\frac{\partial B_y}{\partial y}=0$ |
| | $\frac{\partial B_y}{\partial x}=0$ | $B(y,t)=B_0f(t)b(y)$ | |

The boundary conditions of the magnetic field should be especially explained. For the magnetic diffusion equation, the magnetic induction intensity, which varies with time as function $f(t)$ and with space as function $b(y)$, becomes $B(y,t)=B_0f(t)b(y)$, where $B_0$ represents the amplitude of the magnetic field intensity.

Space function $b(y)$ is the same as the function describing the magnetic induction intensity at the axial of the solenoid. The coefficient $c_{\rm b}$ can be such that the function $b(y)$ varies between zero and one, as shown in Fig. 2:

$$b(y)=c_{\rm b}\Big(\frac{y-a_1}{\sqrt{(y-a_1)^2+r^2}}-\frac{y-a_2}{\sqrt{(y-a_2)^2+r^2}}\Big), \tag{9}$$

where

$$c_{\rm b}=\Big(\frac{a-a_1}{\sqrt{(a-a_1)^2+r^2}}-\frac{a-a_2}{\sqrt{(a-a_2)^2+r^2}}\Big)^{-1}$$

and $a=(a_1+a_2)/2$.

The time function expression $f(t)$ is dependent on the time varying magnetic field, such as the time-harmonic or pulse magnetic field and so on. For example, a triangular pulse expression is expressed as

$$f(t)=\begin{cases} lt/2, nT<t<l/2+nT,\\ -2(t-l)/l, l/2+nT<t<l+nT,\\ \qquad\qquad n=0,1,2,3,\ldots,\\ 0, l+nT<t<(n+1)T, \end{cases} \tag{10}$$

where $l$ is the pulse duration, $n$ is the period number, and $T$ is the period time.

This periodic function is expressed by its Fourier series[11] in the form of

$$f(t) = \frac{1}{4ml} + \sum_{-n}^{+n} c_n \mathrm{e}^{-\mathrm{i}2\pi nt/2ml}, \quad n = 1,2,3,\ldots, \tag{11}$$

where $m$ is equal to $2T/l$ and the coefficient $c_n$ is given by

$$c_n = \frac{1}{T}\int_0^T f(t)\mathrm{e}^{\mathrm{i}2\pi nt/2ml}\,\mathrm{d}t = -\frac{(-1+\mathrm{e}^{\pi n\mathrm{i}/2m})^2 m}{(\pi n)^2}.$$

The curve plotted in Fig. 3(b) shows that the Fourier series in Eq. (11) has exactly the features required by Fig. 3(a).

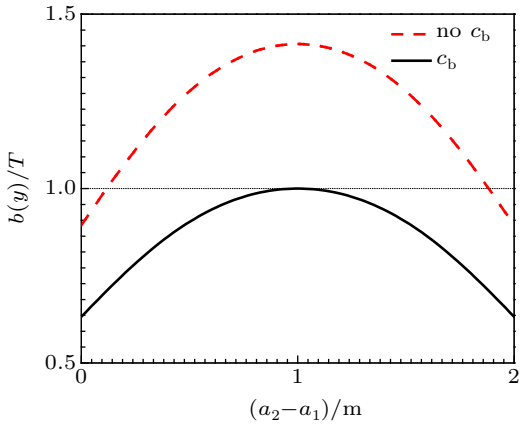



**Fig. 2.** (color online) Variations of the coefficient $c_b$ with $a_2 - a_1$.

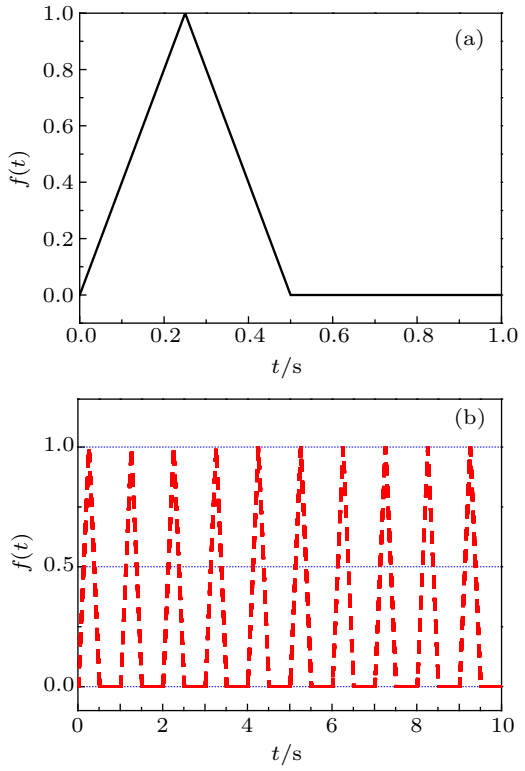



**Fig. 3.** (color online) (a) Theoretical function $f(t)$ during a period and (b) a plot of its variation derived from the Fourier series expansion in Eq. (11) in the case of $m = 1$ and $l = 0.5$ s.

## 3. Numerical details and code validation

### 3.1. Numerical details

The momentum, along with the continuity equation and magnetic diffusion equation are computed numerically by an open source code based on a finite volume method (FVM), as described by Ferziger and Peric.[12] The momentum and continuity equations are solved using the PISO algorithm as shown in Fig. 4. Convergence is defined in the implicit iteration loop when $|(\varphi - \varphi_{\mathrm{old}})/\varphi_{\max}| < 10^{-5}$, where $\varphi$ denotes a solved variable of a cell at the current iteration level, $\varphi_{\mathrm{old}}$ represents the corresponding value at the previous iteration level and $\varphi_{\max}$ is the maximum value of the variable at the current iteration level in the entire domain. It leads to physically incorrect solutions, when $\nabla \cdot \boldsymbol{B} \neq 0$. So it is necessary to correct the magnetic field in order to guarantee that $\nabla \cdot \boldsymbol{B} = 0$ is fulfilled in each time step,[13] as shown in Fig. 5. Similarly, for the velocity correction, one first needs to obtain an intermediate solution $\boldsymbol{B}^*$ and then one can derive a Poisson equation for an auxiliary variable, $\varphi$. From $\nabla^2\phi = \nabla \cdot \boldsymbol{B}^*$, the auxiliary variable $\varphi$ can be calculated; then for the corrected magnetic field $\boldsymbol{B} = \boldsymbol{B}^* - \nabla(\phi)$, the relation $\nabla \cdot \boldsymbol{B} = 0$ will hold.[14]

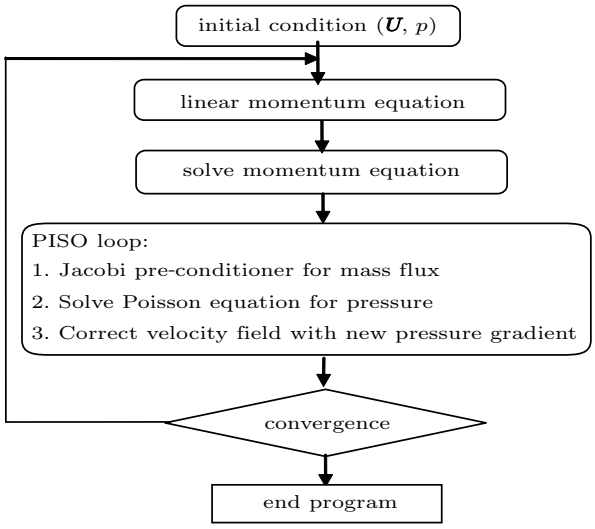



**Fig. 4.** PISO algorithm that can be summarized as the above processes for unsteady flow.

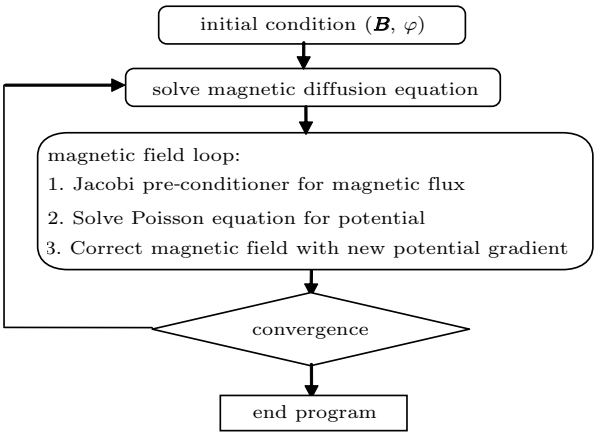



**Fig. 5.** Projection method that can be summarized as the above processes for $\nabla \cdot \boldsymbol{B} = 0$.

### 3.2. Code validation

In order to evaluate the numerical model for an unsteady flow under a time varying magnetic field, a test case is the fluid-flow field in a coreless induction furnace. Kaddah and Szekely[15] compared their results with the experimental results reported by Hunt and Moore.[15] Using the same simulation domain, the initial conditions and physical properties as shown in Table 2, the results from the model in this paper are compared with previous results. The relationship[16] between maximum $B$ and $I$ can be described by the following equation:

$$B_0 = \sqrt{2}\frac{\mu_m NI}{H_c}\left(1+0.88\frac{r_c}{H_c}\right), \tag{12}$$

where $N$, $r_c$, and $H_c$ respectively denote the number of turns, the radius, and the height of the coil.

The simulation domain with height $H_c = 0.3$ m and radius $r_c = 0.15$ is divided into $60 \times 60$ cells. Figure 6 shows the axial velocity, determined in experiments by Hunt and Moore and the numerical results by Szekely, which are compared with the numerical results achieved using the model suggested here at $y = 0.225$ m. The calculated velocities in Fig. 6 are in good agreement with the experiment data. The slight discrepancies from the experiment can be explained by shortcomings of the model or experimental errors. Figure 7 shows that the flow configuration consists of two asymmetrical vertices in a meridian plane. The flow pattern is globally consistent with previous result.

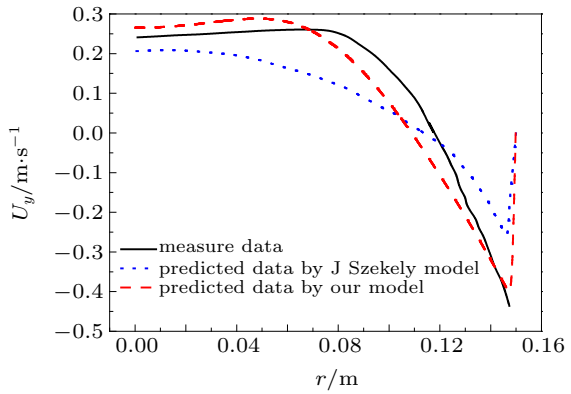



**Fig. 6.** (color online) Comparisons of the numerical results of axial velocity with the measured data and also with the results from Szekely's model.

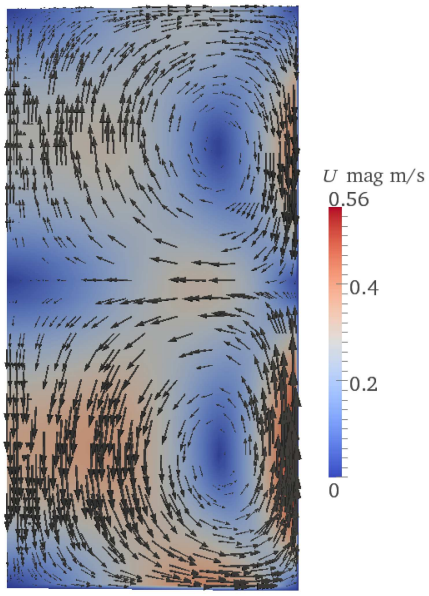



**Fig. 7.** (color online) Velocity vectors of the mercury under time-harmonic magnetic field in a steady state.

## 4. Results and discussion

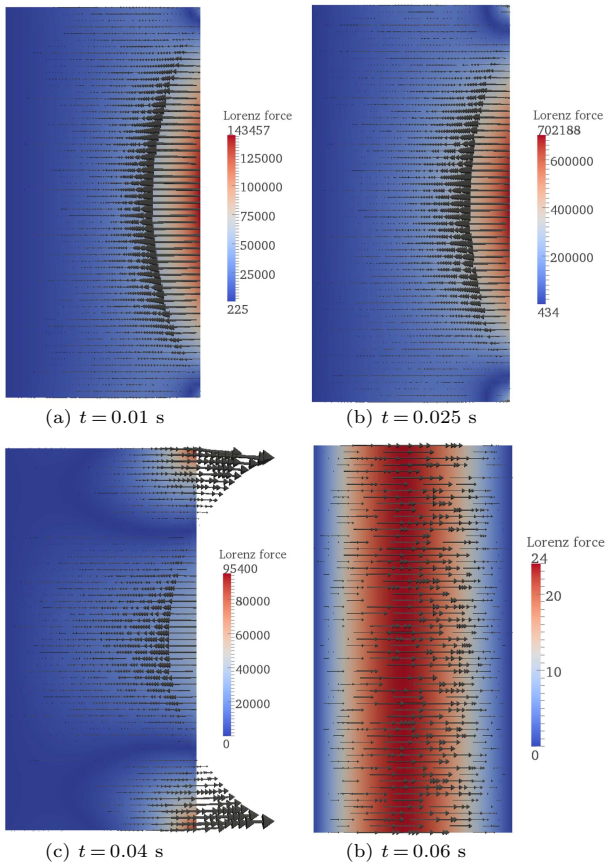
In order to simulate the electromagnetic force and velocity field of molten iron under a PMF, physical parameters are shown in Table 2 and the boundary condition of the magnetic equation at the side wall is $B(y,t) = B_0 f(t) b(y)$, where $b(y)$ is given as Eq. (9), $f(t)$ is the triangular function $f(t)$ that is given by Eq. (10), $B_0$ is 0.3 T, $m = 1$, and $l = 0.05$ s.

**Table 2.** Physical parameters of molten iron and mercury.

| Quantity | Symbol | Hg | Molten iron |
|---|---|---|---|
| Magnetic permeability/(H/m) | $\mu_m$ | $1.257 \times 10^{-6}$ | $1.257 \times 10^{-6}$ |
| Electrical conductivity/(S/m) | $\sigma$ | $1.06 \times 10^{6}$ | $7 \times 10^{5}$ |
| Density/(kg/m$^3$) | $\rho$ | 13268 | 7000 |
| Viscosity/(m$^2$/s) | $\nu$ | $1.24 \times 10^{-7}$ | $8.57 \times 10^{-7}$ |

### 4.1. Pulsed electromagnetic force distribution

The electromagnetic force distribution in a whole pulse period is shown in Fig. 8. In applying a pulse process, the magnitude of the electromagnetic force, whose direction points to the inside of the melt at the middle part and points to the outside of the melt at both the top and bottom end sides, rises at first, peaks and then decreases with variation of the magnetic flux density.




(a) $t = 0.01$ s (b) $t = 0.025$ s

(c) $t = 0.04$ s (b) $t = 0.06$ s

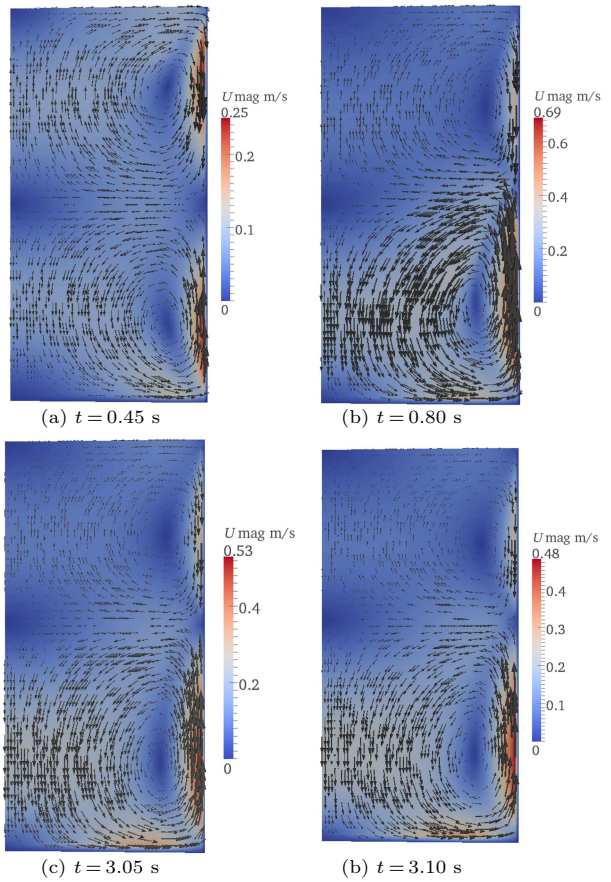
**Fig. 8.** (color online) Electromagnetic force distributions of the melt at different moments during the pulse period (in N/m$^3$).

In the case of no magnetic field process, the direction of the electromagnetic force inversely points to the outside of the melt and the magnitude of the electromagnetic force is far less than that of the force in applying a pulse process. The direction of the electromagnetic force alternately changes in each period, which causes the vibration of the melt at the top surface.

### 4.2. Velocity field under PMF

Figure 9 shows numerical predicted maps of the velocity vector at different times. It is noticeable that the flow configuration consists of two asymmetrical vortices in a meridian plane. The flow pattern is nevertheless globally consistent with previous results.[9] It is easy to interpret accurately the evolution of the flow configuration in a velocity field at different times.

Figure 10 shows the evolution of the melt velocity with time at $G$ point: the liquid velocity first increases and then decreases with time passing by and has a quasi steady state after twenty pulse periods. It is noteworthy that the liquid velocity begins to increase and then decrease in each pulse period. This is because the melt velocity increases with the electromagnetic force. The velocity inversely decreases for viscous drag and turbulent dissipation without electromagnetic force.




(a) $t = 0.45$ s (b) $t = 0.80$ s

(c) $t = 3.05$ s (b) $t = 3.10$ s

**Fig. 9.** (color online) Velocity vectors of molten iron under PMF at different times.

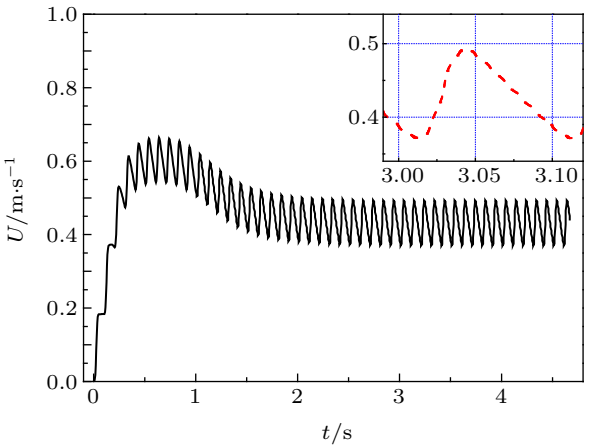



**Fig. 10.** (color online) Velocity magnitude varying with time under PMF at $G$ point ($x = 0.225$ m, $y = 0.1498$ m). The insert shows the velocity varying in one period ($t = 3.00$–$3.10$ s).

## 5. Conclusions

An unsteady MHD model under a time-varying magnetic field is developed and successfully used to simulate a melt flow by coupled transient magnetic-convection conditions. A Fourier series scheme, which can be used for an arbitrary period pulse magnetic field, is employed to implement the periodic boundary of a PMF. A preliminary result is given to illustrate the electromagnetic force distributions and transient velocity field of a molten melt after several periods under a triangular PMF.

## References

[1] Gao Y L, Li Q S, Gong Y Y and Zhai Q J 2007 *Mater. Lett.* **61** 4011
[2] Li Q S, Song C J, Li H B and Zhai Q J 2007 *Mater. Sci. Eng. A* **466** 101
[3] Wang B, Yang Y S, Zhou J X and Tong W H 2008 *Trans. Nonferrous Met. Soc. China* **18** 536
[4] Zi B T, Ba Q X and Cui J Z 2000 *Scr. Mater.* **43** 377
[5] Gong Y Y, Luo J, Jing J X, Xia Z Q and Zhai Q J 2008 *Mater. Sci. Eng. A* **497** 147
[6] Li Y J, Tao W Z and Yang Y S 2012 *J. Mater. Process. Technol.* **212** 903
[7] Kolesnichenko A F, Podoltsev A D and Kucheryavaya I N 1994 *ISIJ Int.* **34** 715
[8] Zi B T, Yao K F, Xu G M and Cui J Z 2003 *Acta Phys. Sin.* **52** 115 (in Chinese)
[9] Ma X P, Yang Y S and Wang B 2009 *Int. J. Heat Mass Transfer* **52** 5285
[10] Davidson P A 2001 *An Introduction to Magnetohydrodynamics* (Cambridge: Cambridge University Press) pp. 117–157
[11] Xiao C Y and Zhang J 2010 *Chin. Phys. B* **19** 120302
[12] Ferziger J H And Peric M 2002 *Computational Methods for Fluid Dynamics*, 3rd edn. (New York: Springer-Verlag) pp. 158–178, 292–296
[13] Brackbill J U and Barnes D C 1980 *J. Comput. Phys.* **35** 426
[14] Chen X W and Shi B C 2005 *Chin. Phys.* **14** 1398
[15] Kaddah N E and Szekely J 1983 *J. Fluid Mech.* **133** 37
[16] Taberlet E and Fautrelle Y 1985 *J. Fluid Mech.* **159** 409